Multiple acoustic diffraction around rigid parallel wide barriers

Hequn Min[a] and Xiaojun Qiu
State Key Laboratory of Modern Acoustics and Institute of Acoustics, Nanjing University, Nanjing 210093, People's Republic of China

(Received 18 September 2008; revised 30 March 2009; accepted 8 May 2009)

A ray-based method is presented for evaluating multiple acoustic diffraction by separate rigid and parallel wide barriers, where two or more neighboring ones are of equal height. Based on the geometrical theory of diffraction and extended from the exact boundary solution for a rigid wedge, the proposed method is able to determine the multiple diffraction along arbitrary directions or at arbitrary receiver locations around the diffracting edges, including the positions along the shadow or reflection boundaries or very close to the edges. Comparisons between the results of the numerical simulations and the boundary element method show validity of the proposed method.
 [DOI: 10.1121/1.3147491]

PACS number(s): 43.50.Gf, 43.20.El, 43.50.Lj [AJMD] Pages: 179–186

I. INTRODUCTION

To assess the impacts of noise on multiple residential buildings along highways, a quantitative description of the multiple sound diffraction over these buildings is required. Sometimes these buildings are similar with same height and the receiving points are close to the top edges of these buildings compared to the wavelength, such as the top floor windows. Separate parallel wide barriers with some neighboring ones of equal height can be considered as the simplified model of such buildings.

Much research has been undertaken on the multiple acoustic diffraction around similar obstacles. Fujiwara *et al.*[1] introduced a technique to estimate the double sound diffraction over one wide barrier by replacing the obstacle with an equivalent thin screen of a certain height, and then the thin screen's noise reduction due to the single diffraction can be evaluated with an empirical formula derived by Kurze and Anderson.[2] Though this technique has been applied to roughly estimate the sound attenuation due to diffraction for engineering purposes,[3,4] it leads to highly erroneous results for diffraction over several obstacles.[5] About 50 years ago, Keller[6–8] presented the geometrical theory of diffraction (GTD) to describe the diffraction. Although the GTD is a geometrical acoustics method, it is accurate for most practical cases when the sound wavelength is smaller than obstacle dimensions.[7] Pierce[5] presented an asymptotic solution and later an exact one together with Hadden[9] to solve the single diffraction around a wedge. He extended that asymptotic solution to evaluate the double-edge diffraction around a single wide barrier[5] based on the concepts of Keller's GTD.[6–8] Although the second-order diffraction term in this double-edge model has been afterwards extended by Chu *et al.*[10] to higher orders for evaluating the diffraction around a wide barrier with finite thickness, Pierce's methods[5,9] mentioned above have not been extended for the separate wide barriers yet.

Kawai[11] developed a method for diffraction around a rigid multi-sided barrier, which was later modified by Kim *et al.*[12] for many extended cases such as multiple wedges or knife edges and polygonal-like shapes. However, for diffracted waves traveling along the shadow or reflection boundaries from the edges, some terms in their methods become infinite, which needs additional complex asymptotic approach to approximate.[13] Additionally these methods require confirming the total field continuity close to each shadow or reflection boundary, which leads to quite complicated computation for the diffraction by several obstacles with more than four edges.

Based on the concepts of Pierce's double-edge model,[5] Salomons[14] presented a model for sound propagation over several wedges in three-dimensional field. In his method, however, both source and receiver are required being far from edges and there are singularities similar to the methods of Kawai[11] and Kim *et al.*[12] for diffraction along the reverse direction of the incident wave on edges.[9,14] Such diffraction occurs commonly around the coplanar edges on top of barriers with same height.

Wadsworth and Chambers[15] modified the Biot–Tolstory–Medwin model[16] for diffraction around single wide barrier or double knife edges in time domain, with both source and receiver far away from the edges also. But the computational load of this model is much greater than that of the frequency domain based solutions such as that of Salomons[14] in most practical cases.[15] Based on the GTD and statistical energy analysis, Reboul *et al.*[17] recently proposed equations able to evaluate the multiple diffraction around several diffracting edges. Nonetheless this method has acceptable accuracy only at relatively high frequencies because it considers the field as the energetic summation of different waves and loses the interference between the waves. Bougdah *et al.*[18] experimentally investigated the acoustic performance of a rib-like structure used for traffic noise control lately, which includes periodically spaced edges or walls, and no theoretical or numerical model on the multiple acoustic diffraction over such structure has been proposed yet.

[a]Author to whom correspondence should be addressed. Electronic mail: hqmin@nju.edu.cn

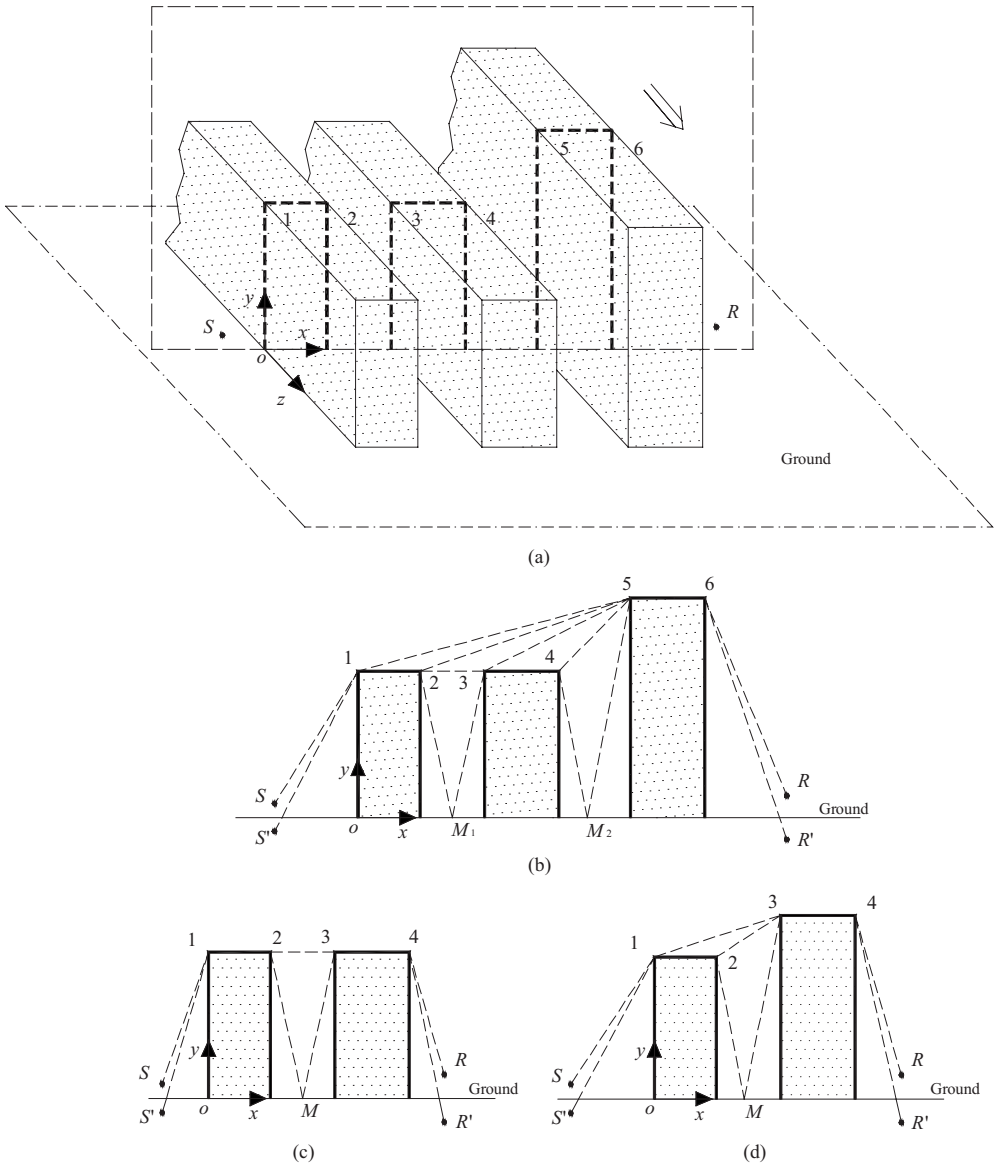

FIG. 1. Typical scenarios of parallel infinitely long wide barriers with source S and receiver R. The dashed lines in (b)–(d) represent the propagation paths of the diffracted waves over barriers. Barrier top edges 1,2,…,6 are diffracting edges. S' and R' are images of S and R to the infinite rigid ground, respectively. M, M_1, and M_2 are ground reflection points of the rays between two barriers. (a) Three-dimensional scenario with three barriers, where two neighboring ones are of equal height. A point source and receiver located in a same plane perpendicular to lengthwise axis of barriers. (b) Cross-section geometry of the scenario in (a). (c) Cross-section geometry with two barriers of equal height. (d) Cross-section geometry with two barriers of different heights.

Despite the previous studies reviewed above, currently there is no appropriate analytical solution for the multiple sound diffraction over a few rigid and parallel wide barriers yet, where some neighboring ones are of equal height. Based on Keller's GTD,[6–8] this paper proposes a method to evaluate the multiple diffraction at arbitrary receiver locations around such obstacles.

II. THEORETICAL METHOD

A typical scenario with three barriers is shown in Fig. 1(a), where two neighboring ones have the same height. Here infinitely long and rigid parallel wide barriers are assumed on the infinite and rigid ground. Right-handed Cartesian coordinates are defined and the origin is located on the intersection line between ground and the leftmost vertical side of the barriers. Only the incident wave normal to axis z (the lengthwise axis of barriers) is considered here. Accordingly the geometry in Fig. 1(a) can be simplified to a plane that is perpendicular to axis z and contains the receiver and source locations as shown in Fig. 1(b). The solution for oblique incidence can be easily obtained from the one for normal incidence with the method mentioned in Ref. 9. When the heights of all barriers are identical, only two barriers of equal height as shown in Fig. 1(c) are analyzed for succinctness.

Based on the GTD method,[6–8] the sound rays that are able to reach a certain receiving point come only from the sources and diffracting edges that can be "observed" from that point. And the multiple sound diffraction is described as individual multiply diffracted waves. Therefore the total sound field at receiver R around the wide barriers comprises the direct rays, the reflected rays, and all the diffracted rays. The direct or reflected rays are determined in the common

way. And the total diffracted field at receiver R with source S, $\phi_{d,\mathrm{tot}}(S,R)$, is the summation of overall diffracted rays coming along all possible diffraction paths[6,8] and is evaluated as

$$\phi_{d,\mathrm{tot}}(S,R) = \sum_{n=1}^{N} \phi_{d,n}(S,R|E_1,E_2,\ldots,E_n), \tag{1}$$

where $\phi_{d,n}(S,R|E_1,E_2,\ldots,E_n)$ represents the field of an individual ray $S \to E_1 \to E_2 \to \cdots \to E_n \to R$, which has been diffracted for n times (orders) and is called an n-order diffracted ray in this paper. E_1, E_2, …, and E_n are, respectively, the edge positions that the n-order diffracted ray propagates along in turn. Accordingly, $\phi_{d,1}(S,R|E_1)$ is the field of a singly diffracted ray and $\phi_{d,2}(S,R|E_1,E_2)$ is the field of a doubly diffracted ray as referred to in previous studies.[11,12] The value N is the considered maximum diffraction orders in the field. In the work presented, it is assumed that every two edges are spaced apart with a sufficiently large distance so that the rays, which are diffracted for two or more times by a same edge, can be neglected,[10,11] for example, the rays $S \to 1 \to 4 \to 1 \to 4 \to R$, $S \to 1 \to 4 \to 1 \to 4 \to 1 \to 4 \to R$, etc., in Fig. 1(c). The numerical results presented in Fig. 5 serve to validate this assumption, where these rays diffracted more than once by a same edge are found to be much weaker than the rays diffracted only once by each edge. Thus an n-order diffracted ray propagates along n different edges and N in Eq. (1) equals the number of all the edges.

A similar case with two wide barriers of different heights shown in Fig. 1(d) is taken as an example to illustrate the search scheme for all the possible diffracted rays reaching R in Figs. 1(b) and 1(c). When there is no ground and each vertical side of the barriers becomes semi-infinite in Fig. 1(d), the diffracted rays reaching R are $S \to 1 \to 2 \to 3 \to 4 \to R$ and $S \to 1 \to 3 \to 4 \to R$ only. After taking the ground reflection into account, ten additional rays appear coming from the images of source or edge 2 over the barriers to the image of receiver. Then the overall rays reaching R in Fig. 1(d) are $S(S') \to 1 \to 2 \to 3 \to 4 \to R(R')$, $S(S') \to 1 \to 2 \to M \to 3 \to 4 \to R(R')$, and $S(S') \to 1 \to 3 \to 4 \to R(R')$, where the letters in the brackets mean optional. S' and R' represent the respective images of the source and receiver to the ground and M is the ground reflection point of the rays from edge 2 to edge 3.

When the heights of these two barriers become identical as shown in Fig. 1(c), it is assumed that every edge can observe all the others and receive rays from all the others at its location. Then in Fig. 1(c) the total number of diffracted rays reaching R is counted as 28, whose details are not presented for concision. Based on cases in Figs. 1(c) and 1(d), the total number of diffracted rays reaching R in Fig. 1(b) is up to 116.

A. Diffraction coefficient

Before the presence of a diffracting edge E_l, the initial sound field at this edge location delivered by the ray $S \to E_1 \to E_2 \to \cdots \to E_l$ is denoted by ϕ_{ini}, where subscript l is an integer. Once the edge E_l is encountered, the initial ray is diffracted and the sound field of the corresponding diffracted

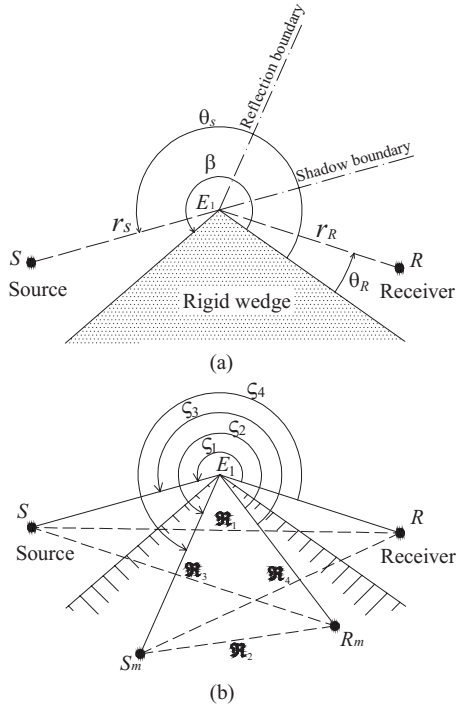

FIG. 2. Cross-section geometry of single diffraction over a rigid wedge whose vertex is edge E_1. (a) Illustration of the locations of source and receiver. θ_S and θ_R are turn angles from right side of wedge to source S and receiver R separately. r_S and r_R are distances in cross-section plane from edge E_1 to source S and receiver R, respectively. Shadow boundary is the extending line of the incident direction from S to E_1, and reflection boundary is the reflected line of the incident direction from S to E_1 due to the source-face of the wedge. (b) Illustration of the parameters ς_i in Eq. (3) and $\Re_i$ in Eq. (5). S_m and R_m are the images of S and R, respectively, to the nearest wedge face. $\varsigma_1 = \angle RE_1S$, $\varsigma_2 = \angle R_mE_1S_m$, $\varsigma_3 = \angle R_mE_1S$, and $\varsigma_4 = \angle RE_1S_m$, where each angle is determined by anticlockwise turning its initial side to its terminate side. Meanwhile $\Re_1 = |RS|$, $\Re_2 = |R_mS_m|$, $\Re_3 = |R_mS|$, and $\Re_4 = |RS_m|$.

ray at the receiving location, ϕ_d, is assumed to be proportional to ϕ_{ini} and can be expressed from the GTD (Refs. 6 and 8) as

$$\phi_d = \phi_{\mathrm{ini}} \cdot D(S \to E_1 \to E_2 \to \cdots \to E_l, R|E_l), \tag{2}$$

where $D(S \to E_1 \to E_2 \to \cdots \to E_l, R|E_l)$ is the complex diffraction coefficient correlated with the diffracting edge E_l, the initial ray to E_l, $S \to E_1 \to E_2 \to \cdots \to E_l$, and the receiver location R. In particular, $D(S \to E_1, R|E_1)$ denotes the diffraction coefficient for a single diffraction and can be simplified as the expression of $D(S,R|E_1)$. It is called the single diffraction coefficient below.

The detailed form of $D(S,R|E_1)$ can be obtained by dividing the singly diffracted field ϕ_d with ϕ_{ini} in Eq. (2), where ϕ_{ini} becomes the direct sound from source and ϕ_d is solved with the Hadden–Pierce solution,[9] which is an exact boundary solution for single diffraction with a point source incidence as shown in Fig. 2(a). Although the Hadden–Pierce solution[9] is only presented for the three-dimensional field, it is used in this paper for both three-dimensional and two-dimensional fields by extracting the free field Green function out of its presented formulas.[9] The deduced single diffraction coefficient is expressed as

$$D(S,R|E_1) = -\frac{\sum_{i=1}^{4} A(\varsigma_i)\cdot F_v(\omega, r_S, r_R, \varsigma_i, \beta)}{\pi \cdot G_f(S|E_1)}, \tag{3}$$

where $G_f(S|E_1)$ denotes the free field Green function in the two-dimensional or the three-dimensional field between two locations S and E_1, indicating the directly incident field at edge E_1, and $F_v(\omega, r_S, r_R, \varsigma_i, \beta)$ is a derived integral

$$F_v(\omega, r_S, r_R, \varsigma_i, \beta) = \int_0^1 I(q)dq, \tag{4}$$

where ω is the angular frequency of the wave, and the parameters r_S and r_R are distances in cross-section plane from edge E_1 to source S and receiver R, respectively. β is the exterior angle of the wedge corresponding to diffracting edge E_1. ς_i are the diffracting turn angles and defined individually as[9] $\varsigma_1 = |\theta_R - \theta_S|$, $\varsigma_2 = 2\beta - |\theta_R - \theta_S|$, $\varsigma_3 = \theta_R + \theta_S$, and $\varsigma_4 = 2\beta - (\theta_R + \theta_S)$, whose constructions are illustrated in Fig. 2(b). The integrand function $I(q)$ in Eq. (4) is[9]

$$I(q) = \begin{cases} e^{jk\Re_i}/\Re_i & \text{for the three-dimensional field} \\ (-j/4)H_0^{\,2}(k\Re_i) & \text{for the two-dimensional field,} \end{cases} \tag{5}$$

where k is the wave number and $j = \sqrt{-1}$.

The parameter $\Re_i$ is defined as distance between two points where the turn angle anticlockwise encircling the diffracting edge from one point to another is ς_i, which is illustrated in Fig. 2(b) and depends on the integrant q in Eq. (4) by[9]

$$\Re_i = [L^2 + r_R r_S (Y - Y^{-1})^2]^{1/2}, \tag{6}$$

in which

$$Y = \left[\frac{\tan(A(\varsigma_i)) + \tan(qA(\varsigma_i))}{\tan(A(\varsigma_i)) - \tan(qA(\varsigma_i))}\right]^{\beta/(2\pi)}. \tag{7}$$

$A(\varsigma_i)$ is an angular function and can be expressed as

$$A(\varsigma_i) = \frac{\pi}{2\beta}(-\beta - \pi + \varsigma_i) + \pi U(\pi - \varsigma_i) \tag{8}$$

and

$$U(\theta) = \begin{cases} 1 & \text{if } \theta \geq 0 \\ 0 & \text{if } \theta < 0. \end{cases} \tag{9}$$

The quantity L in Eq. (6) is defined as the total distance along the path of diffracted ray from S to edge E_1 and then to R, which equals $r_S + r_R$ in Fig. 2(a).

In particular, when receiver R is located on the shadow boundary or the reflection boundary of E_1 shown in Fig. 2(a) with ς_1 or ς_4, respectively equaling π and then the corresponding $A(\,)$ becoming $\pi/2$, Eq. (4) leads to singularities and cannot be used to calculate $F_v(\,)$ due to the singular values of Y with Eq. (7) and then those of $\Re_1$ or $\Re_4$, respectively, with Eq. (6). Under these situations, $\Re_i$ for Eq. (5) can be calculated by using its geometrical definition as

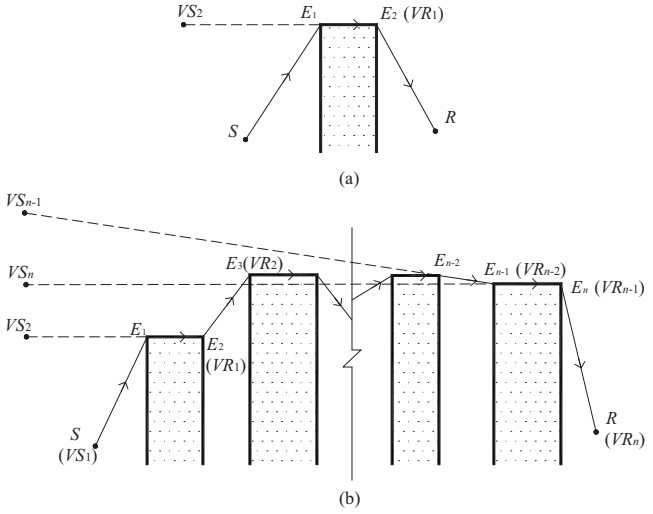

FIG. 3. Illustration of one individual diffracted ray over wide barriers. (a) One generic doubly diffracted ray by edges E_1 and E_2 over a single wide barrier whose width is not less than one wavelength. (b) One generic n-order diffracted ray over several wide barriers from source S to receiver R by edges E_1, E_2, $E_3, \ldots, E_{n-1}$, and E_n in turn. VS_n is a virtual source for edge E_n, VR_{n-1} is a virtual receiver for edge E_{n-1}, and so on.

$$\Re_i = (r_S^{\,2} + r_R^{\,2} - 2r_S \cdot r_R \cdot \cos\varsigma_i)^{1/2}, \tag{10}$$

which results $r_S + r_R$ for $\Re_i$ when $\varsigma_i = \pi$. The function $I(q)$ from Eq. (5) now becomes independent of integrant q in Eq. (4) and accordingly

$$F_v(\omega, r_S, r_R, \pi, \beta) = G_f(r_S + r_R). \tag{11}$$

B. Doubly diffracted ray

In Fig. 3(a), a general doubly diffracted ray is investigated, which is diffracted by E_2 with the initial ray $S \to E_1 \to E_2$. The latter ray can be treated as a singly diffracted ray by edge E_1 with location E_2 being a virtual receiver defined as VR_1 as if the edge E_2 does not exist. Then the field of the ray $S \to E_1 \to E_2$ at edge E_2 can be denoted by $\phi_{d,1}(S, VR_1|E_1)$. Following Eq. (2), the field at receiver R by doubly diffracted ray $S \to E_1 \to E_2 \to R$, $\phi_{d,2}(S, R|E_1, E_2)$, can be determined by

$$\phi_{d,2}(S,R|E_1,E_2) = \phi_{d,1}(S,VR_1|E_1)\cdot D(S \to E_1 \to E_2, R|E_2), \tag{12}$$

where $D(S \to E_1 \to E_2, R|E_2)$ is the diffraction coefficient correlated with the diffracting edge E_2, the initial ray $S \to E_1 \to E_2$, and receiver R. Meanwhile the singly diffracted field $\phi_{d,1}(S, VR_1|E_1)$ can also be obtained with Eq. (2) as

$$\phi_{d,1}(S,VR_1|E_1) = G_f(S|E_1)\cdot D(S,VR_1|E_1), \tag{13}$$

where the initial field at edge E_1 is the direct sound field, $G_f(S|E_1)$.

From the GTD (Refs. 6–8) and Pierce's ray-based approach,[5] the generic diffraction coefficient in Eq. (2) can be approximately evaluated with the specific one for a single diffraction in Eq. (3). For the ray $S \to E_1 \to E_2 \to R$, the diffraction by edge E_2 can be viewed as a single diffraction by assuming that the sides of wedge E_2 become semi-infinite

and the initial ray comes from a virtual source VS_2 illustrated in Fig. 3(a). Here VS_2 locates on the reverse extension line of $E_1 \rightarrow E_2$ and is apart from E_2 for a distance equaling the total length of the initial ray $S \rightarrow E_1 \rightarrow E_2$. Then $D(S \rightarrow E_1 \rightarrow E_2, R|E_2)$ in Eq. (12) can be determined as

$$D(S \rightarrow E_1 \rightarrow E_2, R|E_2) = D(VS_2, R|E_2) \cdot \alpha(E_1, E_2), \quad (14)$$

where $D(VS_2, R|E_2)$ is a single diffraction coefficient and can be calculated with Eq. (3). $\alpha(E_1, E_2)$ is a weighting factor introduced to avoid the redundant counting of the reflection on the connecting side between two edges E_1 and E_2 and is unit if E_2 is separated from E_1. In Fig. 3(a) the weighting factor equals 1/2,[5,10] where E_2 and E_1 are connected with a side whose width is greater than one wavelength. Further details for determining the weighting factor can be found in Ref. 10, which developed an interpolation method to determine the weighting factor for two successive arbitrarily spaced and connected edges.

Thus the field at R delivered by the given doubly diffracted ray, $\phi_{d,2}(S, R|E_1, E_2)$, can be rewritten by substituting Eqs. (13) and (14) into Eq. (12) as

$$\phi_{d,2}(S, R|E_1, E_2) = G_f(S|E_1) \cdot D(S, VR_1|E_1) \cdot D(VS_2, R|E_2) \cdot \alpha(E_1, E_2), \quad (15)$$

which is a product of the direct sound field at the first diffracting edge E_1, the diffraction coefficients, and the weighting factor correlated with the two edges.

C. Generic equations for the individual *n*-order diffracted ray

Similarly, $\phi_{d,n}(S, R|E_1, E_2, E_3, \ldots, E_{n-1}, E_n)$, the sound field of a generic n-order diffracted ray over several wide barriers shown in Fig. 3(b), can be evaluated by multiplying the direct sound field at edge E_1 with the diffraction coefficients and weighting factors at the n diffracting edges,

$$\phi_{d,n}(S, R|E_1, E_2, E_3, \ldots, E_{n-1}, E_n) = G_f(S|E_1) \cdot \prod_{l=1}^{n} D(VS_l, VR_l|E_l) \cdot \alpha(E_{l-1}, E_l), \quad (16)$$

where

$$\alpha(E_{l-1}, E_l) = \begin{cases} 1 & \text{if the edges } E_{l-1} \text{ and } E_l \text{ are separated} \\ 1/2 & \text{if the edges } E_{l-1} \text{ and } E_l \text{ are connected.} \end{cases} \quad (17)$$

In Eq. (16), VR_l denotes the virtual receiver from edge E_l as illustrated in Fig. 3(b), which is the location of E_{l+1}, the next edge along the diffraction ray path. VS_l denotes the virtual source to edge E_l and locates on the reverse extension line of $E_{l-1} \rightarrow E_l$, apart from E_l for a distance equaling the total length of the ray $S \rightarrow E_1 \rightarrow E_2 \rightarrow \cdots \rightarrow E_l$. In fact VS_l, VR_l, and edge E_l construct a complete geometry for a single diffraction at wedge E_l. Particularly, VS_1 represents the location of source S, VR_n represents the location of receiver R, and $\alpha(E_0, E_1) \equiv 1$.

When two or more neighboring barriers have same height, the barriers' configuration in Fig. 3(b) becomes equivalent to that in Fig. 1(b) and 1(c). This causes that the virtual receiver VR_l correlated with edge E_l locates on the shadow boundary or reflection boundary of VS_l for some diffraction rays. For example, in the propagation of ray $S \rightarrow 1 \rightarrow 2 \rightarrow 3 \rightarrow 4 \rightarrow R$ in Fig. 1(c), the virtual receiver VR_2 (edge 3) locates on the shadow boundary of initial ray $S \rightarrow 1 \rightarrow 2$ to edge 2. Under such a situation, the integral term in $D(VS_l, VR_l|E_l)$ can be evaluated with Eq. (11) to avoid singularities. Additionally, receiver R may be located on edge E_n in Fig. 3(b), which causes that $r_R = 0$ and the parameter θ_R fails to be assigned for evaluating $D(VS_n, VR_n|E_n)$ with Eq. (3). In such case, the n-order diffracted ray actually degrades to one with $(n-1)$ orders, $S \rightarrow E_1 \rightarrow E_2 \rightarrow \cdots \rightarrow E_{n-1} \rightarrow E_n$. Accordingly the field $\phi_{d,n}(S, R|E_1, E_2, E_3, \cdots, E_{n-1}, E_n)$ can be replaced with $\phi_{d,n-1}(S, E_n|E_1, E_2, E_3, \cdots, E_{n-1})$, which avoids the evaluation difficulty from $r_R = 0$. There is no other limit of r_R and θ_R for diffraction coefficient evaluation with Eq. (3) and the field at arbitrary receiver locations can be explicitly calculated with Eq. (13), even when receivers are quite close to the diffracting edge compared with the wavelength.

It is worth noting that the method proposed in Eq. (16) depends on the assumption from Eqs. (14) and (17) that the edge-edge distances, $|E_l E_{l+1}|$, are greater than one wavelength. That is, in principle, the proposed method works as well as the GTD with the edge-edge distances larger than the wavelength.

The proposed method is validated with numerical simulations to investigate its accuracy and applicability. The presentation of results is facilitated with insertion loss (IL), which is defined as

$$\text{IL} = 20 \log_{10}(|P_{\text{tot},0}|/|P_{\text{tot},t}|), \quad (18)$$

where $P_{\text{tot},0}$ is sound pressure in the total field at receiver without the barriers while $P_{\text{tot},t}$ is the one with the barriers.

III. RESULTS AND DISCUSSIONS

When there is only a single wide barrier or double parallel knife edges, which are discussed abundantly in the previous studies,[5,10–12,14,15] the method of Eq. (16) reduces to a double-edge form of Eq. (15). Preliminary numerical comparisons in such cases between the proposed method and the previous models, such as the models of Pierce,[5] Chu *et al.*,[10] Kawai or Kim *et al.*,[11,12] and Wadsworth *et al.*,[15] have been

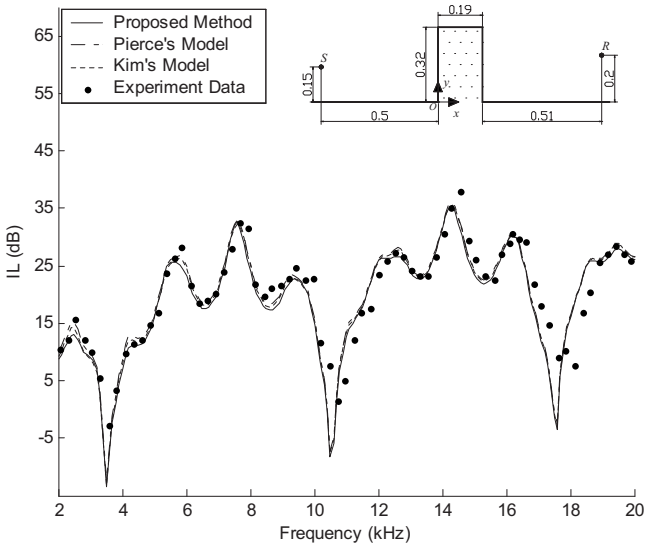

FIG. 4. The IL spectra of a rigid single barrier with width of 0.19 m and height of 0.32 m in the three-dimensional field, where a point source is located at S (−0.5 m, 0.15 m, 0 m) and receiver is R (0.7 m, 0.2 m, 0 m). The unit of the illustrated geometry in the inset figure is meter. The solid line represents the predicted results with the proposed method (proposed method). The dashed-dotted line and dotted line represent the predictions with Pierce's model (Ref. 5) (Pierce's model) and those with the models of Kim *et al.* (Ref. 12) (Kim's model), respectively. The solid points are experimental data from study by Wadsworth and Chambers (Ref. 15) (experimental data).

carried out. Only the results from a three-dimensional case with a rigid single wide barrier are presented in Fig. 4 for succinctness. The corresponding inset figure shows the cross-section geometry. In Fig. 4, good agreements are observed among the predicted results and the experimental data, which serve to validate the proposed method for predicting the double-edge diffraction on the other hand. Additionally, computations have been carried out in advance to investigate how weak the rays diffracted more than once by a same edge in comparison with the rays diffracted only once at each edges. In this case, energy amplitudes of rays $S\rightarrow1\rightarrow2\rightarrow1\rightarrow2\rightarrow R$, $S\rightarrow1\rightarrow2\rightarrow1\rightarrow2\rightarrow1\rightarrow2\rightarrow R$, and $S\rightarrow1\rightarrow2\rightarrow1\rightarrow2\rightarrow1\rightarrow2\rightarrow1\rightarrow2\rightarrow R$ are compared to that of the ray $S\rightarrow1\rightarrow2\rightarrow R$. Figure 5 presents the corresponding results of the energy magnitude ratio, where the wavelength at frequency 1820 Hz equals the barrier width. From Fig. 5, the rays diffracted for two, three, and four times at a same edge are, respectively, weaker than the ray diffracted only once at each edge by 30, 60, and 90 dB at least. Although the magnitude ratios increase a little when the barrier width is smaller than one wavelength, the rays diffracted twice or more by a same edge are sufficiently weak to be neglected in the proposed method.

For the current problem of several wide barriers with some neighboring ones of equal height, since it is hard to use the previous analytical models to calculate the sound field, the boundary element method (BEM) is employed for numerical validation.[12,14,17] To ensure high numerical accuracy, discretization in the BEM is executed by quintic boundary elements with the largest length smaller than one fifteenth of the considered smallest wavelength.

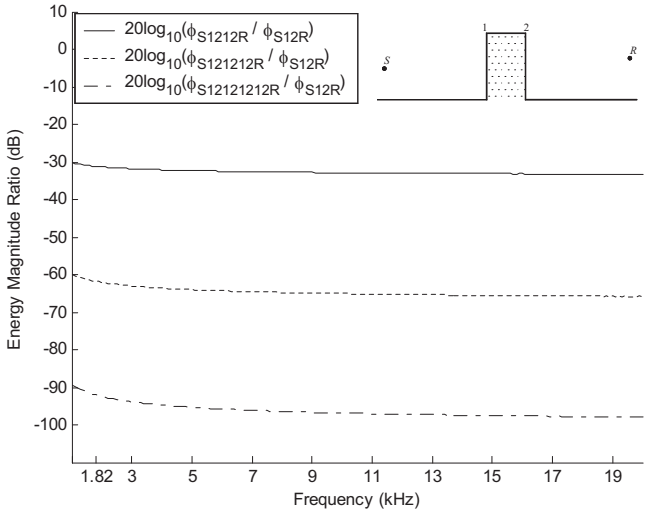

FIG. 5. The spectra of energy magnitude radio of the rays $S\rightarrow1\rightarrow2\rightarrow1\rightarrow2\rightarrow R$, $S\rightarrow1\rightarrow2\rightarrow1\rightarrow2\rightarrow1\rightarrow2\rightarrow R$, and $S\rightarrow1\rightarrow2\rightarrow1\rightarrow2\rightarrow1\rightarrow2\rightarrow1\rightarrow2\rightarrow R$ that are diffracted twice or more by a same edge, compared to the ray $S\rightarrow1\rightarrow2\rightarrow R$ that is diffracted only once at each edge. The location of source, receiver, and two edges are illustrated in the inset figure. The parameter ϕ_{S1212R} represents the sound pressure amplitude of ray $S\rightarrow1\rightarrow2\rightarrow1\rightarrow2\rightarrow R$, ϕ_{S12R} represents that of ray $S\rightarrow1\rightarrow2\rightarrow R$, and so on.

Two numerical cases whose geometries correspond to those in Figs. 1(c) and 1(b), respectively, are investigated with typical dimensions of barriers in the two-dimensional field. In the first case shown in the inset figures of Figs. 6 and 7, two parallel rigid barriers with identical width of 0.6 m and the same height of 2.4 m are spaced from 1 m on the infinite rigid ground. A coherent line source parallel to lengthwise axis is defined and located at S (−3.2 m, 0.4 m), while receivers are chosen at R (2.37 m, 2.3 m) in Fig. 6 apart from the nearest edge for 0.2 m (equaling wavelength at frequency 1720 Hz) and at (5.14 m, 0.5 m) in Fig. 7 apart

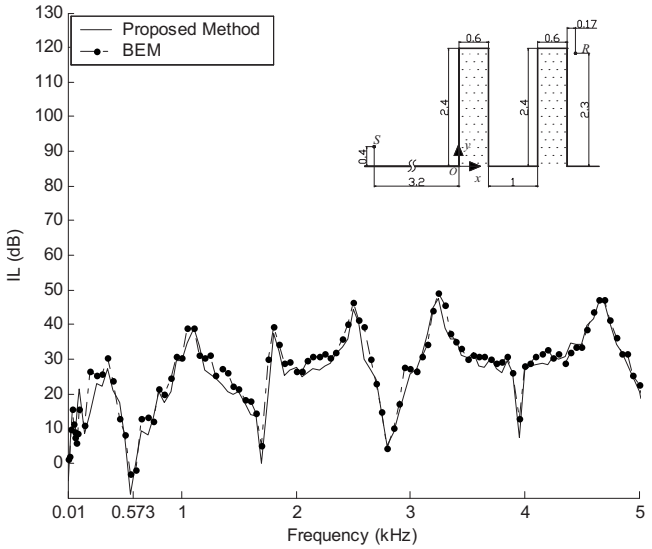

FIG. 6. The spectra of IL at receiver R (2.37 m, 2.3 m), which is in the shadow zone of source S (−3.2 m, 0.4 m) due to two rigid barriers with a same height of 2.4 m blocking the incidence. The barriers have identical width of 0.6 m and are spaced for 1 m. The unit of the illustrated geometry in the inset figure is meter. The solid line represents the predicted results with the proposed method (proposed method) and the dashed-dotted line represents the numerical results from the BEM.

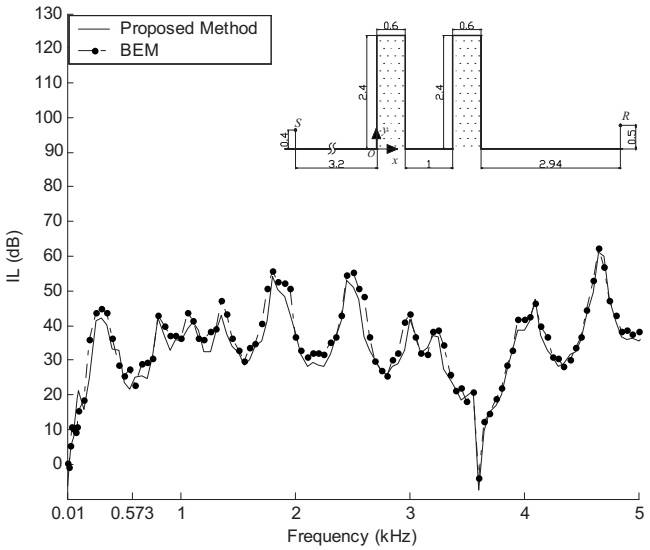

FIG. 7. Same caption as Fig. 6 except that location of R changes to (5.14 m, 0.5 m).

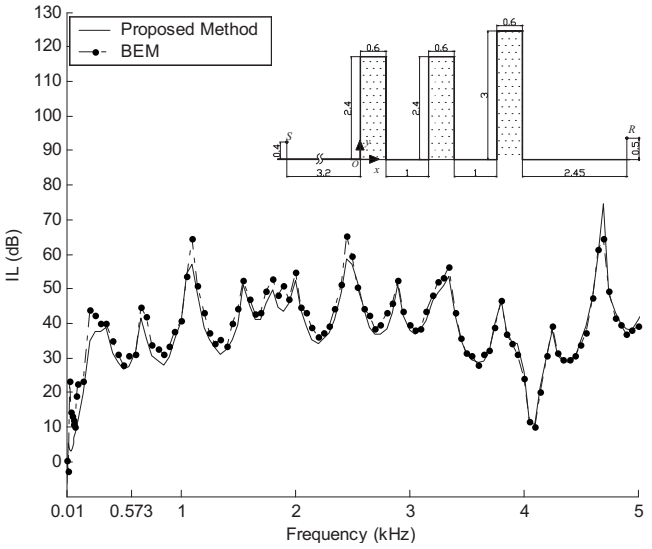

FIG. 9. Same caption as Fig. 8 except that location of R changes to (6.25 m, 0.5 m).

from the nearest edge for 3.5 m (equaling wavelength at frequency 98 Hz). Such choice of receiver locations allows the investigation on sound field in different areas of interest, being close or far from the diffracting edges compared to the wavelength.

The second case is shown in the inset figures of Figs. 8 and 9 with three barriers, where barrier widths remain 0.6 m and the barrier-barrier spaces remain 1 m. In this case, two neighboring barriers have same height of 2.4 m while the other is 3 m high. The definition of source is same as the first case but the receiver locations change to R (3.97 m, 2.9 m) in Fig. 8 and to (6.25 m, 0.5 m) in Fig. 9 based on the same relevant consideration in the first case. In both cases, receivers are in the shadow zone of source due to barriers blocking and either source or receivers can only observe the nearest edge, respectively.

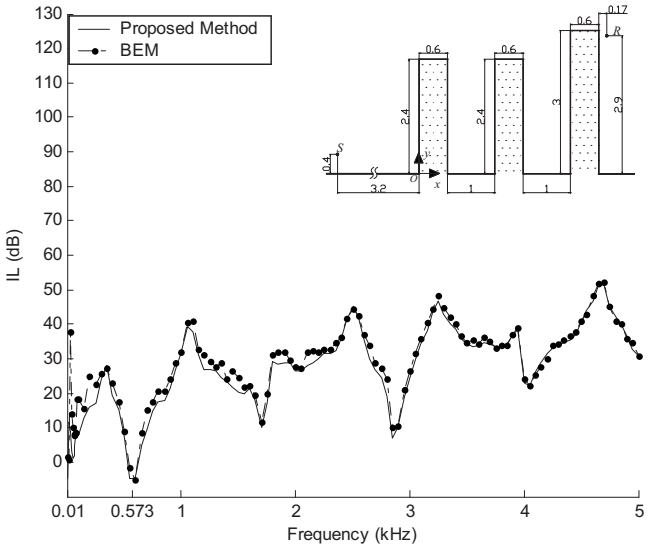

FIG. 8. The spectra of IL at receiver R (3.97 m, 2.9 m) in the shadow zone of source S (−3.2 m, 0.4 m) due to three rigid barriers blocking the incidence, where heights of two barriers are 2.4 m and the other is 3 m high. The barriers have identical width of 0.6 m and are spaced for 1 m one by one. The unit of the illustrated geometry in the inset figure is meter. The solid line represents the predicted results with the proposed method (proposed method) and the dashed-dotted line represents the numerical results from the BEM.

In the case with two barriers, the maximum diffraction order is 4 and the total number of diffracted rays reaching R is 28 considered with the proposed method. The corresponding evaluated IL spectra are shown in Figs. 6 and 7 with receiver locations (2.37 m, 2.3 m) and (5.14 m, 0.5 m), respectively. Here the minimum edge-edge distance is 0.6 m equaling the wavelength at frequency 573 Hz. From Figs. 6 and 7, over the frequencies range from one to eight times larger than 573 Hz, the predictions from the proposed method agree well with those from the BEM, except small discrepancies at some frequencies, whose reasons are not completely clear yet. Moreover, it is found in Figs. 6 and 7 that at frequencies around 573 Hz the agreement between the results with these two methods remains good. The IL curves in Figs. 6 and 7 are quite complex with large fluctuations over the broad frequency range, because of interference between the different waves diffracted by the barriers and reflected from the ground.[19]

Figures 8 and 9 show the corresponding IL spectra for the case of three barriers with receiver locations being (3.97 m, 2.9 m) and (6.25 m, 0.5 m), respectively, where the maximum diffraction orders become 6 and the total number of the diffracted rays reaching R increases up to 116. In this case, the minimum edge-edge distance remains 0.6 m, which is the wavelength at 573 Hz. In Figs. 8 and 9, over the frequency range higher than 573 Hz, the results with the proposed method and those with the BEM are in good agreement again, except small discrepancies at some frequencies. Additionally, at the frequencies around 573 Hz in Figs. 8 and 9, the agreement between the predictions with these two methods is found to be good also.

The computational times with these two methods in both cases are compared. A total of 9800 quintic elements are considered at the highest frequency of 5 kHz in the BEM for both numerical cases. And it takes over 1 h by a personal

computer with a 2.4 GHz Intel Q6600 processor and 4 Gbytes of random access memory to execute the BEM evaluation at such single frequency. The evaluation with the proposed method takes only 1.4 min in the first case and 7.9 min in the second case on the same computer for a single frequency and the corresponding computational time is frequency independent. This indicates that for an equivalent accuracy degree, the proposed method is much faster than the BEM.

From the above results, the proposed method can evaluate the multiple acoustic diffraction over wide barriers more efficiently than the BEM. As a ray-based method, the accuracy of the method for evaluating the individual diffracted rays depends on the geometry dimensions compared to the wavelength, which are edge-edge distances in the current problem. The results of the numerical simulations show that the method is accurate when the edge-edge distances are larger than one wavelength. It is also found that the method remains accurate even when the edge-edge distances become a little less than the wavelength. Furthermore, though the method in Eq. (16) is proposed for wide barriers, it can be used in principle to evaluate the individual multiply diffracted rays around parallel knife edges also, for example, around the rib-like structure studied by Bougdah *et al.*[18]

IV. CONCLUSION

In this paper, a ray-based method is developed to solve the multiple acoustic diffraction around parallel wide barriers with some neighboring ones of equal height. The method is based on Keller's GTD (Refs. 6–8) and extended from Pierce's exact boundary solution[5] for a rigid wedge. The proposed method can avoid singularities while solving multiple diffraction along the shadow boundaries or the reflection boundaries. Numerical simulations show that the method can predict the field at arbitrary receiver locations.

The accuracy and applicability of the method are validated numerically with the BEM in the two-dimensional field where the model was shown to be considerably accurate when the edge-edge distances are larger than one wavelength. The proposed method has more computational efficiency than the BEM and is useful for predicting acoustic diffraction along arbitrary directions or at arbitrary receiver locations around parallel barriers with various configurations.

ACKNOWLEDGMENTS

The authors are grateful to the anonymous reviewers for their constructive comments on improving the original manuscript. Projects 10674068 and 10604030 supported by NSFC.

[1]K. Fujiwara, Y. Ando, and Z. Maekawa, "Attenuation of a spherical sound wave diffracted by a thick plate," Acustica **28**, 341–347 (1973).
[2]U. J. Kurze and G. S. Anderson, "Sound attenuation by barriers," Appl. Acoust. **4**, 35–53 (1971).
[3]D. A. Bies and C. H. Hansen, *Engineering Noise Control: Theory and Practice*, 2nd ed. (E & FN SPON, London, 1996).
[4]RAYNOISE user's manual, version 3.1 LMS, Numerical Technologies (2002).
[5]A. D. Pierce, "Diffraction of sound around corners and over wide barriers," J. Acoust. Soc. Am. **55**, 941–955 (1974).
[6]J. B. Keller, "Diffraction by an aperture," J. Appl. Phys. **28**, 426–444 (1957).
[7]J. B. Keller, "Diffraction by an aperture. II," J. Appl. Phys. **28**, 570–579 (1957).
[8]J. B. Keller, "Geometrical theory of diffraction," J. Opt. Soc. Am. **52**, 116–130 (1962).
[9]W. J. Hadden and A. D. Pierce, "Sound diffraction around screens and wedges for arbitrary point source location," J. Acoust. Soc. Am. **69**, 1266–1276 (1981).
[10]D. Chu, T. K. Stanton, and A. D. Pierce, "Higher-order acoustic diffraction by edges of finite thickness," J. Acoust. Soc. Am. **122**, 3177–3193 (2007).
[11]T. Kawai, "Sound diffraction by a many-sided barrier or pillar," J. Sound Vib. **79**, 229–242 (1981).
[12]H. S. Kim, J. S. Kim, H. J. Kang, B. K. Kim, and S. R. Kim, "Sound diffraction by multiple wedges and thin screens," Appl. Acoust. **66**, 1102–1119 (2005).
[13]R. G. Kouyoumjian and P. H. Pathak, "A uniform geometrical theory of diffraction for an edge in a perfectly conducting surface," Proc. IEEE **62**, 1448–1461 (1974).
[14]E. M. Salomons, "Sound propagation in complex outdoor situations with a non-reflecting atmosphere: Model based on analytical solutions for diffraction and reflection," Acust. Acta Acust. **83**, 436–454 (1997).
[15]G. J. Wadsworth and J. P. Chambers, "Scale model experiments on the insertion loss of wide and double barriers," J. Acoust. Soc. Am. **107**, 2344–2350 (2000).
[16]H. Medwin, E. Childs, and G. M. Jebsen, "Impulse studies of double diffraction: A discrete Huygens interpretation," J. Acoust. Soc. Am. **72**, 1005–1013 (1982).
[17]E. Reboul, A. L. Bot, and J. P. Liaudet, "Radiative transfer equation for multiple diffraction," J. Acoust. Soc. Am. **118**, 1326–1334 (2005).
[18]H. Bougdah, I. Ekici, and J. Kang, "A laboratory investigation of noise reduction by riblike structures on the ground," J. Acoust. Soc. Am. **120**, 3714–3722 (2006).
[19]D. Duhamel, "Efficient calculation of the three-dimensional sound pressure field around a noise barrier," J. Sound Vib. **197**, 547–571 (1996).